10.21611/qirt.2022.2011
16th Quantitative InfraRed Thermography Conference

IR Thermal and UV imaging characterization of melanocytic lesions

by C. Magalhaes* **, J. Mendes* ** and R. Vardasca* ***

* LABIOMEP, INEGI, Rua Dr. Roberto Frias 400, 4200-465 Porto, Portugal
** Faculdade de Engenharia, Universidade do Porto, Rua Dr. Roberto Frias S/N, 4200-465 Porto, Portugal, up201607752@up.pt
*** ISLA Santarém, Largo Cândido dos Reis, 2000-241 Santarém, Portugal

Abstract

The deadliest form of skin cancer, melanoma, is frequently confused with its benign version, melanocytic nevus. Diagnosis is based on visual assessment, requiring commonly tumour excision for confirmation. Infrared thermal (IRT) imaging has shown its potential to assist diagnosis innocuously, but richer tissue characterization might be sustained with additional methods, as ultraviolet (UV) imaging. In this study, IRT and UV imaging were combined to assess 31 melanocytic lesions. Relevant differences were found for IRT parameters (up to 3 C) being UV features also meaningful for lesion characterization (p-value 0.05). Future application of findings would supply complementary information, assisting in harmless premature detection.

Keywords: infrared thermal imaging, ultraviolet imaging, skin cancer, melanocytic lesions

1. Introduction

Skin cancer is one of the most common types of neoplastic conditions, being categorized as melanoma and non-melanoma, according to its cell-type of origin [1]. The former is the most harmful type of malignant skin tumours, being its late detection associated to a survival rate lower than 15% [2]. The existing diagnosis lays on lesion inspection and monitoring over a period of months/years that is normally followed by an excisional biopsy at the suspicion of malignancy, as this pigmented tumour is often mistaken with its benign sibling, melanocytic nevus [3,4].

Over the last years, there was a relying in dermoscopy for detecting melanoma prematurely and avoid purposeless biopsies. The extensive years of training necessary to correctly identify melanocytic lesions complicate the attainment of this aim [5,6], mainly due to large visual resemblances between melanoma and melanocytic nevus, as the diagnostic process rests solely on very specific anatomical patterns [3]. Thus, the quest for a non-invasive imaging method continues to ensure premature quality detection without unnecessary pain and scaring.

Apart from visual aspects, affected malignant regions display different metabolic alterations when compared to benign areas [7]. The affected systems, e.g., vascular and nervous, cause changes in blood perfusion to the lesion site, having an impact in heat transfers [8] 6LQFH LQIUDUHG FDPHUDV DOORZ WKH FDSWXULQJ RI WKHUPDO (IRT) imaging could be a good candidate to collect data related to this physiological process [8,9]. IRT imaging has shown its potential in previous research as a diagnostic tool for this type of skin neoplastic condition, in a contactless and innocuous manner [10]. Thermal cameras are able to mirror skin temperature patterns representative of physiological processes related to the development of different skin tumours. Thus, basing the diagnosis in functional parameters as opposed to visual ones [11–13]. When implemented it in a dynamic mode, physiological activity is even more emphasized due to skin stimulation, as oppose to what is verified when a static approach is preferred. [13]. Nonetheless, to fully characterize the tissue under evaluation, different imaging methods can be combined. Ultraviolet (UV) radiation is usually associated to skin cancer lesions as a causing agent instead of a diagnostic resource [14,15]. However, irradiation of an object with an UV-light source (300-400 nm) results in black and white images where lighter areas represent regions of light reflection and darker areas show locations of absorption. Hence, it can be useful in characterizing skin lesion patterns that are unseen with standard visible-light imaging [16,17]. The fact that it allows an in-vivo, non-invasive examination of skin tissue sustains the idea that this imaging technique could be a candidate of interest as an adjuvant tool for skin cancer diagnosis. The use of UV radiation for skin cancer assessment is hardly mentioned in the literature, appearing barely in fluorescence studies [18]. To the best of achieved knowledge, applications of UV imaging for skin cancer assessment are inexistent.

In this study, static and dynamic IRT imaging and UV imaging were combined to assess melanoma and melanocytic nevi. Several thermal and UV parameters were retrieved and evaluated as possible candidates for the identification of malignant and benign pigmented lesion cases.

2. Methodology

Thermal and UV images were collected at Instituto Português de Oncologia do Porto Francisco Gentil, E.P.E.. Ethical approval was requested and given before approaching patients to participate in this research. The study's population group included cooperative individuals with at least one possible melanoma or melanocytic nevus lesion. Some exclusion criteria were defined as necessary precautions before image acquisition, namely, ingestion of alcoholic or caffeinated beverages and/or heavy meals, smoking 2 hours prior, partake in tiring physical activities, non-removal of jewellery items or application of ointments to the leased area. All participants were of legal age and able to read, understand and sign the informed consent. The lesions were previously diagnosed by a physician of the Plastic and Reconstructive Surgery department. All diagnoses were confirmed by histopathological analysis.

The thermal camera FLIR (Wilsonville, OR, USA) E60sc, previously calibrated with blackbody ISOTECH HYPERION R 982 (Figure 1A and 1B), was used to collect lesion thermograms. Ambient temperature (22.3 ± 0.9°C) and relative humidity (47.3 ± 1.8°C) were monitored with TESTO 175H1 hygrometer to guarantee optimal conditions for thermal recordings [13,19]. All patients, equipment and examination room followed the guidelines of Glamorgan protocol [19]. Thermal stimulation was performed using an aluminium medal (diameter=50 mm, thickness=20 mm, thermal conductivity=237 $W.cm^{-1}.K^{-1}$ at 298.2 K) (Figure 1C) through direct contact (conduction). UV images were collected with prototype camera Nurugo Smart UV, coupled to a smartphone (Samsung S20). As images were collected indoors, an attachment with a UV lamp (range of 350 to 390 nm) was mounted on the UV camera and used as an external light source during image collection (certified by CE, FCC, KC and IEC [20]) (Figure 1D).

Fig. 1. *Material for thermal and UV evaluation of skin neoplasm: a) Thermal imaging camera FLIR E60sc, b) blackbody ISOTECH HYPERION R model 982, c) aluminium medal, d) Nurugo Smart UV camera and UV lamp attachment.*

After acclimatization to examination room (10 min), thermal recording begun with the collection of a static thermogram (T_X). Cold stimulus was then applied for 1 minute and a new lesion thermogram was captured immediately after (T_0). Subsequent images were collected at the 15, 30 and 45 second and 1, 2, 3, 4 and 5 minute time-mark after thermal stimulation. Thus, the 5-minute recovery period was represented by 8 thermograms (T_15, T_30, T_45, T_1, T_2, T_3, T_4 and T_5). The UV image was captured after thermal collection to assure that no thermal disruption was provoked by the momentaneous UV irradiation that occurs during UV image capture. In total, 31 lesions were evaluated being 20 melanoma and 11 melanocytic nevi.

Thermal and UV images were analysed using a Python programming script [21]. For IRT image analysis, thermograms were firstly converted to *.mat* files using FLIR ThermaCAM Researcher Professional 2.10 software package. After image loading, tumour centre was selected, and the lesion was cropped with a 40x40 window (Figure 2A). T_X was used to construct a thermal profile based on temperature values stored in the main diagonals of lesion area (Figure 2B). The values of each diagonal were multiplied to compute an average temperature profile that would best represent the tumour under analyses (Figure 2C). Dynamic analysis followed for all thermograms, having the static analysis as base. The goal was to compute the maximum temperature difference (D) between the centre of the lesion (20x20 region) and its periphery (Figure 2D). Thus, if the lesion showed a hypothermic profile, the lowest average temperature of a 5-pixel area inside the 20x20 region was searched, while the highest temperature of a 5-pixel area was searched in its surroundings, and their difference was calculated (Figure 2E). The opposite was performed if the tumour showed an hyperthermic tendency. The average temperature of the 40x40 region and its standard deviation (std) were also computed and stored for all images.

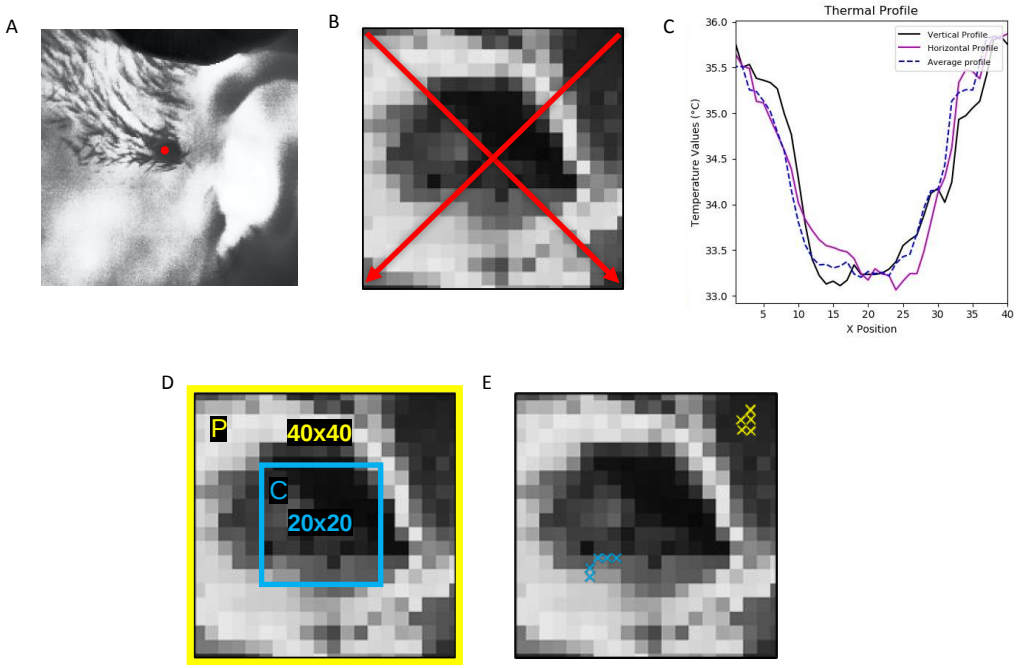

Fig. 2. *Scheme of IRT image analysis: A-selection of lesion centre, B-cropping of 40x40 region and collection of temperature values, C-temperature profiles, D-division in central (C) and peripheral (P) areas for dynamic analysis, E-selection of 5-pixel areas with highest and lowest average temperature.*

UV analysis also started with lesion centre selection and cropping of a 100x100 region of interest (ROI) (Figure 3A and 3B). Normalized and equalized histograms of ROI were computed (Figure 3C and 3D), and the following features were retrieved from each histogram: maximum/minimum pixel intensity in ROI (max/min_int), number of pixels with maximum/minimum intensity (max/min_pixels), skewness and kurtosis. Additionally, the raw histogram was smoothed with a FIR filter and the number of grayscale intensity peaks was recorded (Figure 2D).

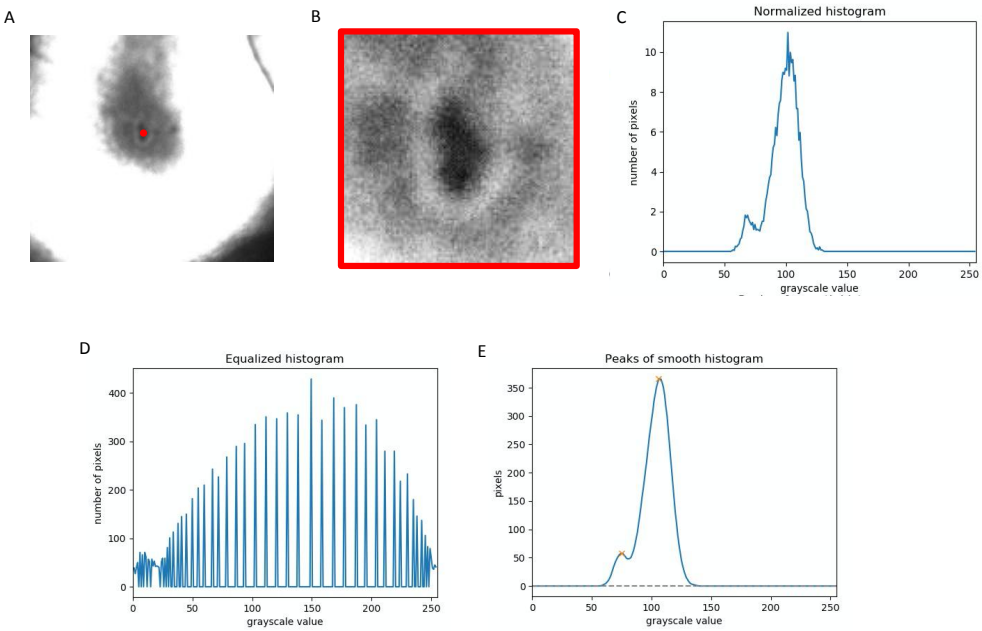

Fig. 3. *Scheme of UV image analysis: A-selection of lesion centre, B-cropping of 100x100 region, C-normalized histogram of ROI, D-equalized histogram of ROI, E-smooth histogram with grayscale intensity peaks (marked with orange crosses).*

The parameters retrieved from thermal and UV analysis were used as variables for the non-parametric statistical tests U-Mann Whitney and Kruskal Wallis, with SPSS software, to verify if any of the collected variables were influenced by neoplasm type. Thus, being possible candidates for neoplasms differentiation. A significance level of 0.05 was used for both tests.

3. Results and Discussion

The average static thermal profile of melanocytic nevi displayed a slight depression when approaching lesion centre, while melanoma exhibited an almost imperceptible hump (Figure 4A). Although these tendencies have been described before as more pronounced curves [10], particularly for most of the melanoma cases assessed here, the static profile appeared as a straight line. This could possibly be the indication of an early-stage tumour, whose identification might be hard when no stimulus is involved. The statistic tests supported these findings, as no static thermal profile value was considered meaningful for lesion distinction (Table 1). Contrarily, on the dynamic assessment, great differences were found between melanoma and nevi tumours (Figure 4B), especially at minute 1 of recovery (Figure 4B). Maximum temperature difference increased greatly for melanomas immediately after cooling (Figure 4B – moments D0 and D15), slightly decreasing after, until the 5-minute time mark. The behaviour of melanocytic nevi was very erratic during minute 1, making the parameter D greater than zero at moments D0, D30 and D1 to D5 and close to zero at DX, D15 and D45. This could indicate that the temperature of some nevi lesions differed from its periphery immediately after cooling, while others only started recovery a few seconds later or even at the 1-minute time mark. Nonetheless, maximum temperature difference was always lower for the benign tumour type, when compared to its malignant sibling. The average temperature of melanoma remained higher than the one of melanocytic nevi during recordings, even after cooling (Figure 4C), sustaining the idea that greater physiological activity is found in this malignant tumour sites and ultimately contributes for a temperature increase. The same was found for std of lesion temperature (Figure 4D). This finding was expected as per verified in dynamic thermal recordings and corroborated by the elaborated thermal profiles; melanoma lesion centres were almost always characterized by thermal values that differed greatly from its surroundings (Figure 4D).

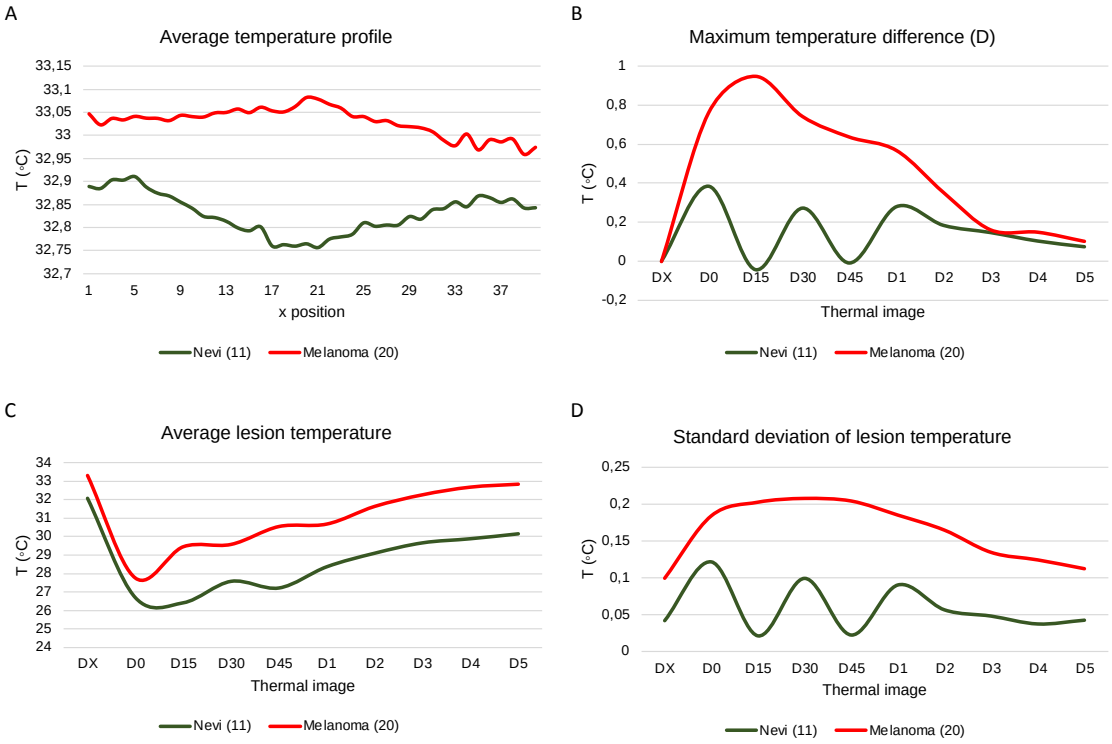

Fig. 4. *IRT imaging results: A-average thermal profile, B, C and D-maximum temperature difference, average lesion temperature and standard deviation of lesion temperature during image acquisition.*

These goes in accordance with the statistical results since almost all maximum temperature difference values until the 1-min time mark and all std values of ROI were considered influenced by lesion type (Table 1).

Table 1. *Collected variables influenced by neoplasm type for U-Mann Whitney and Kruskal-Wallis's test.*

Non-parametric test	Variables influenced by neoplasm type
U-Mann Whitney	D0, D15, D3, max_int (equalized histogram), max_int (normalized histogram), min_int (normalized histogram), min_pixels (normalized histogram), all average values of ROI except at X and 0, all std values of ROI
Kruskal-Wallis	D0, D15, D30, D45, D3, max_int (equalized histogram), max_int (normalized histogram), min_int (normalized histogram), min_pixels (normalized histogram), all average values of ROI except at X and 0, all std values of ROI

Some of the retrieved UV parameters also seemed to sustain the differentiation of melanoma and melanocytic nevi lesions, as number of pixels verified at maximum intensity (Table1 and Figure 5A and B). It is important to note that, even though skewness and kurtosis were not considered relevant by the statistical test for melanoma and melanocytic nevi differentiation, their p-values were close to the significance level established (0.05), ranging between 0.053 and 0.074, thus the visual difference verified in Figure 5C, D, E and F. Overall, the nevi values tended to be higher than the melanoma ones for all parameters (Figure 5).

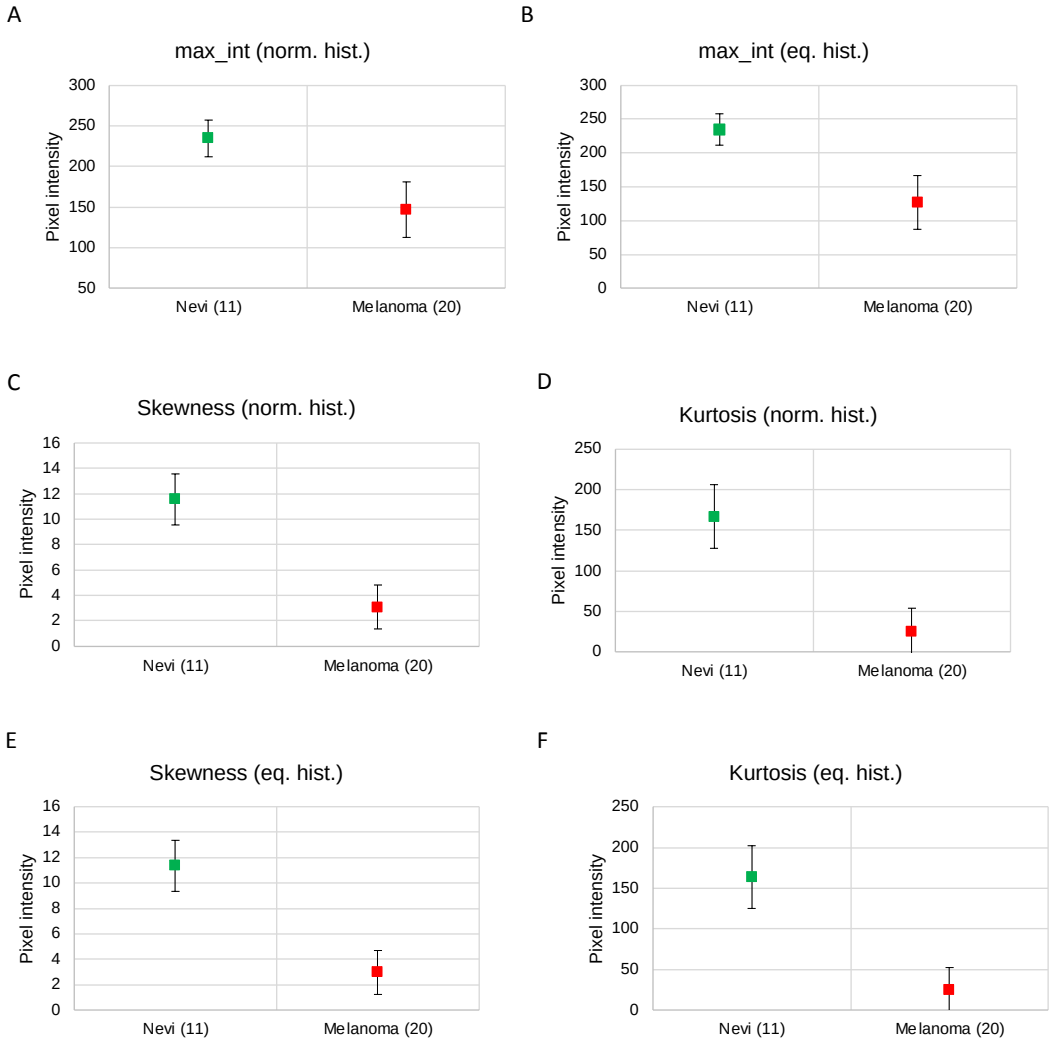

Fig. 5. *UV imaging results: A and B- maximum pixel intensity in ROI for normalized and equalized histogram, C and D- skewness and kurtosis for normalized histogram, E and F-skewness and kurtosis for equalized histogram.*

Since UV images can supply information related to the textural aspect of skin tissue, these results can be clarified by the following. Melanocytic nevi tend to have a more uniform distribution of melanocytes, normally resulting in its homogeneous accumulation in a given area. Hence, the resulted histogram is expected to have a great number of pixels with the same grayscale value. Secondly, the image histogram will likely display an accumulation of pixels towards a darker grey area, being asymmetrical and consequently presenting an elevated value for skewness, as opposed to being more spread with multiple levels of grey across the histogram, as it would happen in a melanoma lesion that is normally characterized by an uneven distribution of melanocytes and a more rugged texture. Ultimately, kurtosis will be greater for melanocytic nevi lesions, as its main peak would be higher than the melanoma one, as a results of the accumulation of a great number of pixels with the same grayscale value.

4. Conclusion

In this study, static and dynamic IRT and UV imaging were combined with the aim of identifying possible features discriminative of benign and malignant melanocytic lesions. The analysed thermal patterns showed greater distinction of melanoma and melanocytic nevi for dynamic variables, particularly during the first minute of recovery. Likewise, some UV parameters also revealed to be of great help for differentiation of melanoma and melanocytic nevi lesions, as maximum intensity verified at normalized and equalized histograms. Thus, indicating the utility of IRT imaging as an innocuous lesion assessment method, particularly if assisted by an additional imaging method, as UV imaging. To sustain this assumption, more images are being collected with the aim of bringing statistical meaning to this hypothesis.

For future work, the retrieved parameters are expected to be used as inputs for a machine learning assistive system intended to aid in the diagnosis process.

Acknowledgments: This research was funded by Project LAETA [grant numbers UIDB/50022/2020, UIDP/50022/2020]; and the PhD Scholarship supported by FCT (national funds through Ministério da Ciência, Tecnologia e Ensino Superior (MCTES)) and co-funded by ESF through the Programa Operacional Regional do Norte (NORTE 2020) (EU funds)) [grant number SFRH/BD/144906/2019].

REFERENCES

[1] P.C. Nasca, H. Pastides, Basic Terminology - Benign and Malignant Neoplasms, in: Fundam. Cancer Epidemiol., Aspen Publishers. Inc., 2001: pp. 23–38. https://books.google.pt/books?id=ggpziP3VEzYC&pg=PA25&dq=malignant+and+benign+neoplasms&hl=pt-PT&sa=X&redir_esc=y#v=onepage&q=malignant and benign neoplasms&f=false (accessed September 21, 2017).

[2] A. Lideikaitė, J. Mozūraitienė, S. Letautienė, Analysis of prognostic factors for melanoma patients, Acta Medica Litu. 24 (2017) 25–34. https://doi.org/10.6001/actamedica.v24i1.3460.

[3] C. Conforti, R. Giuffrida, R. Vezzoni, F.S.S. Resende, N. Meo, I. Zalaudek, Dermoscopy and the experienced clinicians, Int. J. Dermatol. 59 (2020) 16–22. https://doi.org/10.1111/ijd.14512.

[4] R.A. Schwartz, Skin Cancer: Recognition and Management, 2nd ed., Blackwell Publishing, Newark, New Jersey, 2008.

[5] C. Fink, H.A. Haenssle, Non-invasive tools for the diagnosis of cutaneous melanoma, Ski. Res. Technol. (2017) 1–11. https://doi.org/10.1111/srt.12350.

[6] D. Piccolo, A. Ferrari, K. Peris, R. Daidone, B. Ruggeri, S. Chimenti, Dermoscopic diagnosis by a trained clinician vs. a clinician with minimal dermoscopy training vs. computer-aided diagnosis of 341 pigmented skin lesions: a comparative study, Br. J. Dermatol. 147 (2002) 481–486. https://doi.org/10.1046/j.1365-2133.2002.04978.x.

[7] L. V Crowley, Neoplastic Disease, in: An Introd. to Hum. Dis. Pathol. Pathophysiol. Correl., 9th ed., Jones and Bartlett Learning, 2013: pp. 192–209. https://books.google.pt/books?redir_esc=y&hl=pt-PT&id=Tye_Y5gs2pIC&q=neoplastic+disease#v=snippet&q=neoplastic disease&f=false (accessed September 21, 2017).

[8] I.A. Nola, D. Kolanc, Thermography in biomedicine, in: 2015 57th Int. Symp. ELMAR, IEEE, 2015: pp. 17–20. https://doi.org/10.1109/ELMAR.2015.7334485.

[9] C. Herman, The role of dynamic infrared imaging in melanoma diagnosis, Expert Rev. Dermatol. 8 (2013) 177–184. https://doi.org/10.1586/edm.13.15.

[10] C. Magalhães, R. Vardasca, J. Mendes, Recent use of medical infrared thermography in skin neoplasms, Ski. Res. Technol. 00 (2018) 1–5. https://doi.org/https://doi.org/10.1111/srt.12469.

[11] E.F.J. Ring, K. Ammer, Infrared thermal imaging in medicine, Physiol. Meas. 33 (2012) R33–R46. https://doi.org/10.1088/0967-3334/33/3/R33.

[12] M. Pirtini Çetingül, H.E. Çetingül, C. Herman, Analysis of transient thermal images to distinguish melanoma from dysplastic nevi, in: R.M. Summers, B. van Ginneken (Eds.), 2011: p. 79633N. https://doi.org/10.1117/12.877858.

[13] E. Ring, K. Ammer, The technique of infrared imaging in medicine, in: Infrared Imaging, IOP Publishing, 2015: pp. 1–10. https://doi.org/10.1088/978-0-7503-1143-4ch1.

[14] R. Gordon, Skin cancer: An overview of epidemiology and risk factors, Semin. Oncol. Nurs. 29 (2013) 160–169. https://doi.org/10.1016/j.soncn.2013.06.002.

[15] D.L. Narayanan, R.N. Saladi, J.L. Fox, Ultraviolet radiation and skin cancer, Int. J. Dermatol. 49 (2010) 978–986. https://doi.org/10.1111/j.1365-4632.2010.04474.x.

[16] L. Boyers, C. Karimkhani, R. Gamble, R. Dellavalle, Novel and promising sun safety interventions: UV photography and shade structures, OA Dermatology. 9 (2014) 1–6. http://www.oapublishinglondon.com/images/article/pdf/1412792286.pdf.

[17] B.A. Richards, D. Ph, Digital Reflected-Ultraviolet Imaging, (2006) 18–20.

[18] S. Arroyo-Camarena, J. Domínguez-Cherit, L. Lammoglia-Ordiales, D.A. Fabila-Bustos, A. Escobar-Pio, S. Stolik, A. Valor-Reed, J. de la Rosa-Vázquez, Spectroscopic and Imaging Characteristics of Pigmented Non-Melanoma Skin Cancer and Melanoma in Patients with Skin Phototypes III and IV, Oncol. Ther. 4 (2016) 315–331. https://doi.org/10.1007/s40487-016-0036-9.

[19] K. Ammer, The Glamorgan Protocol for recording and evaluation of thermal images of the human body, Thermol. Int. 18 (2008) 125–129.

[20] Nurugo Smart UV camera, (2019). https://en.nurugo.com/products/nurugo_smartuv.php#tab-description.

[21] P. Raybaut, Spyder-documentation, (2009). Pythonhosted. Org.